American College of Neuropsychopharmacology

www.nature.com/npp

ARTICLE

Check for updates

Phenazopyridine promotes *RPS23RG1/Rps23rg1* transcription and ameliorates Alzheimer-associated phenotypes in mice

Chong Wang[1,3]✉, Yuan Zhang[1,3], Dongdong Zhao[2], Yuanhui Huo[2], Jieru Xie[1], Xian Zhang[2], Hong Luo[2], Huaxi Xu[2] and Yun-wu Zhang[2]✉

Alzheimer's disease (AD) is the most common form of dementia with no effective treatment options. A complete elucidation of its underlying molecular mechanisms, including the transcription regulation of genes critically involved in AD, may shed light on new therapeutic development. *RPS23RG1* is a newly identified AD-associated gene, whose expression is decreased in AD and restoration can attenuate AD-like phenotypes in animal models. However, the transcription regulation of *RPS23RG1* remains unknown. In this study, we explored the promoter of *RPS23RG1* and identified its transcription initiation site (TSS) at 1525 bp upstream of the ATG translation start codon. Progressive deletion analysis determined the presence of a negative regulatory region and a positive regulatory region within nucleotide positions +1127 to +1187 and +732 to +1127 relative to the TSS (+1), respectively. We conducted a reporter system to screen for compounds that increase *RPS23RG1* expression through antagonizing its negative regulatory elements and identified phenazopyridine. Importantly, we demonstrated that phenazopyridine not only promoted *RPS23RG1/Rps23rg1* expression, but also reduced AD-like pathologies and cognitive impairments in the APP/PS1 AD model mice. We also determined a critical negative regulatory domain of *RPS23RG1* within nucleotide positions +1177 to +1187 and found that the transcription factor SMAD3 bound to this domain. Inhibition of SMAD3 promoted *RPS23RG1* expression. Moreover, phenazopyridine reduced SMAD3 binding to the *RPS23RG1* promoter without affecting SMAD3 phosphorylation and nuclear localization. Taken together, our results determine the transcription regulation mechanism of *RPS23RG1* and show that phenazopyridine has potential for AD treatment through regulating *RPS23RG1* transcription.

Neuropsychopharmacology; https://doi.org/10.1038/s41386-022-01373-7

INTRODUCTION

Alzheimer's disease (AD) is a neurodegenerative disease and the primary cause of dementia. Two classical pathological hallmarks of AD are the extracellular amyloid plaques and the intracellular neurofibrillary tangles [1–3]. Amyloid plaques comprise deposits of β-amyloid (Aβ) peptides, which are produced from β-amyloid precursor protein (APP) through sequential proteolytic cleavages mediated by β-secretase and γ-secretase [4]. Aβ peptides vary in length and are widely believed to be the primary culprit for AD pathogenesis. Among the species of Aβ, oligomeric $Aβ_{1–42}$ is considered most likely to induce synaptic/neuronal loss and memory deficits in AD [3, 5, 6]. Neurofibrillary tangles consist of hyperphosphorylated forms of the microtubule-associated protein tau. CDK5 and GSK-3β are two major kinases responsible for tau hyperphosphorylation that also causes neurotoxicity in AD [7]. Clinically, AD is characterized by progressive memory loss, cognitive impairments, and eventual inability for daily task performance [8, 9]. Unfortunately, so far there are no effective therapeutic options available. A complete elucidation of the molecular and cellular mechanisms underlying AD pathogenesis should identify targets for developing new AD treatment strategies [10].

RPS23RG1 (ribosomal protein S23 retroposed gene 1) is a transmembrane protein abundantly expressed in the central nervous system [11, 12]. RPS23RG1 can regulate both Aβ generation and tau phosphorylation through modulating the adenylyl cyclase/cAMP/PKA/GSK-3β pathway and the CDK5/p35 complex [11, 13, 14]. Moreover, RPS23RG1 maintains synaptic function through interacting with post-synaptic density components PSD-93 and PSD-95 and thus preventing PSD-93 and PSD-95 from proteasome-mediated degradation [12]. Importantly, RPS23RG1 expression is found decreased in postmortem human AD brain and brain from various AD mouse models [12, 14, 15]; and overexpression of RPS23RG1 and its functional domains can alleviate AD-like behavioral and pathological phenotypes in AD model mice [11, 12, 14, 15]. These findings indicate an important role of RPS23RG1 dysregulation in AD. However, transcription regulation of the *RPS23RG1* gene remains unknown.

In the present study, we explored the promoter of the *RPS23RG1* gene and identified the core region for its transcription regulation. Moreover, we found that phenazopyridine could promote *RPS23RG1/Rps23rg1* expression and attenuate AD-like phenotypes in an AD mouse model.

[1]Department of Basic Medical Sciences, School of Medicine, Xiamen University, Xiamen 361102 Fujian, PR China. [2]Xiamen Key Laboratory of Brain Center, The First Affiliated Hospital of Xiamen University, and Fujian Provincial Key Laboratory of Neurodegenerative Disease and Aging Research, Institute of Neuroscience, School of Medicine, Xiamen University, Xiamen 361102 Fujian, PR China. [3]These authors contributed equally: Chong Wang, Yuan Zhang. ✉email: wangchong@xmu.edu.cn; yunzhang@xmu.edu.cn

Received: 13 March 2022 Revised: 5 June 2022 Accepted: 22 June 2022
Published online: 11 July 2022

MATERIALS AND METHODS

Reagents and antibodies

Phenazopyridine and the SMAD3 inhibitor SIS3 were purchased from MedChemExpress (Monmouth Junction, NJ, USA). Approved Drug Screening Library containing 1600 FDA-approved drugs was from Target Molecule (Wellesley Hills, MA, USA). The monoclonal antibody targeting mouse RPS23RG1 was generated by Sino biological Inc. as reported previously [12]. Antibodies against phosphorylated tau (199), phosphorylated tau (404), phosphorylated GSK-3β, phosphorylated SMAD3, SMAD3, PSD-95, p35, and β-actin are from Cell Signaling Technology (Danvers, MA, USA). Antibodies against total tau (TAU-5) and phosphorylated tau (S202/T205, AT8) are from Thermo Fisher Scientific (Waltham, MA, USA). The antibody against GAPDH is from Abways (Shanghai, China). The antibody against APP (22c11) is from MilliporeSigma (Burlington, MA, USA).

Constructs and transfection

RPS23RG1 promoter fragments were obtained by PCR using the following primers. Various reporter constructs were generated by inserting these fragments into a pGL3-basic vector (Promega, Madison, WA, USA) using an EasyGeno Assembly Cloning kit (TIANGEN, Beijing, China). The constructs were transfected into SH-SY5Y cells using Lipofectamine 2000 (Thermo Fisher Scientific) following the manufacturer's instructions.

Primers used:

Forward −1509: 5′-CCTCTCCTACTGCTTGCCCA-3′;
Forward −506: 5′-TCTCCTGCCTCAACCTCCC-3′;
Forward +732: 5′-CGGGGATCGCTCGTGG-3′;
Forward +1127: 5′-CTTTAGGGGCCTGTCGGGTTGGGA-3′;
Forward +1187: 5′-GGCAGGAATCTTACATCTAGAACTTG-3′;
Forward +1400: 5′-TGCCAGGATGGAGAGGAGAC-3′;
Reverse −506: 5′-AATCGGTTGAACCCAGGAGG-3′;
Reverse +732: 5′-GAGGAGAGCCGCGGCC-3′;
Reverse +1127: 5′-GCTGCCTGTGTTCCGTGC-3′;
Reverse +1156: 5′-CCGCACTCCCAACCCG-3′;
Reverse +1167: 5′-AAGACCCCTCCCCGCAC-3′;
Reverse +1177: 5′-TTTCCCCCAGAAGACC-3′;
Reverse +1187: 5′-CCATGTCTCCTTTCCCCCA-3′;
Reverse +1298: 5′-TCTTGGCGCTTGTCATCAAT-3′;
Reverse +1535: 5′-ATGGGGACATCCAAGGTGAG-3′.

Cell culture and stable cell lines

Human SH-SY5Y and U-87 and mouse N2a cells were cultured in Dulbecco's modified Eagle's media (Hyclone, Logan, UT, USA) supplemented with 10% fetal bovine serum (HyClone) and 1% penicillin/streptomycin (HyClone) and maintained in a humidified incubator with 5% CO_2 at 37 °C. Two *RPS23RG1* promoter fragments (+732/+1127 or +732/+1187) were cloned into a pGL4.17 vector (Promega) and transfected into SH-SY5Y cells. Stable cell lines expressing the reporter construct were derived by limiting dilution and G418 (400 μg/ml, Sangon Biotech, Shanghai, China) selection.

5′-rapid amplification of cDNA ends (RACE)

The 5′ end of human *RPS23RG1* mRNA was identified by 5′-RACE using the SMARTer RACE 5′/3′ Kit (Clontech Laboratories, Inc., Mountain View, CA, USA) following the manufacturer's instructions. Briefly, total RNAs from human SH-SY5Y cells were isolated by the E.Z.N.A. Total RNA Kit I (Omega Bio-Tek, Norcross, GA, USA). First-Strand cDNA Synthesis, RACE, and infusion cloning of the RACE products to the pRACE vector were performed using the reagents provided in the SMARTer RACE 5′/3′ Kit. The following *RPS23RG1* gene-specific primer was used: 5′-GATTACGCCAAGCTTGGGGG TGCCGGCCACTTTGACTG-3′. DNA sequencing was performed to identify the recombinant clones.

Luciferase activity assay

Luciferase activities of the plasmids containing *RPS23RG1* promoter deletion fragments were detected by a Dual-Luciferase® Reporter Assay System (Promega) following the manufacturer's instructions. SH-SY5Y cells were transfected with indicated firefly luciferase reporter plasmids together with a pRL Renilla luciferase reporter plasmid (Promega) for 24 h. Firefly luciferase activity was normalized to Renilla luciferase activity. Luciferase activity of the stable cell lines treated with various drugs was detected by a Steady-Glo® Luciferase Assay System (Promega) following the manufacturer's instructions.

Drug screening

Stable cell lines expressing pGL4.17 vectors containing +732/+1127 or +732/+1187 fragments were used for drug screening. A total of 1600 FDA-approved drugs from Approved Drug Screening Library were tested. First, the +732/+1187 cell line was treated with each drug (10 μM, in triplicate) for 12 h. Equal volume of vehicle was used as a control. The luciferase activities were examined as described above. Then the 732/+1127 cell line was treated with the drugs that increased the +732/+1187 cell line luciferase activity by more than 1.1-fold. The drugs that increased the +732/+1187 cell line luciferase activity by more than 1.2-fold and changed the +732/+1127 cell line luciferase activity with less than 1.1-fold were regarded as potential candidates.

Quantitative real-time PCR

Total RNA extraction, reverse transcription, and PCR were performed using the E.Z.N.A. Total RNA Kit I (Omega Bio-Tek), the RT Master Mix for qPCR (MedChemExpress) and the GoTaq qPCR Master Mix (Promega), respectively. PCR reactions were performed using a fluorescence quantitative PCR system (Applied Biosystems, California, USA) with the following program: 95 °C for 10 min, followed by 40 cycles of 95 °C for 15 s and 60 °C for 1 min. Melting curves were acquired to ensure specific amplification. The primer pairs used for real-time PCR were: RPS23RG1 Homo F (5′-AGGGATGCA GAAGACAGGATTG-3′), RPS23RG1 Homo R (5′-AGTTCGCTTTCAGGTTGTCA-3′); Rps23rg1 Mus F (5′-TGTTGCATACACATACATGC-3′), Rps23rg1 Mus R (5′-TCATTAAGAACGGGAAGAAG-3′); β-actin Homo F (5′-ATCAAGATCATTGCT CCTCCTGAG-3′), β-actin Homo R (5′-CTGCTTGCTGATCCACATCTG 3-′); β-actin Mus F (5′-AGCCATGTACGTAGCCATCC-3′), and β-actin Mus R (5′-CTC TCAGCTGTGGTGGTGAA-3′).

Enzyme linked immunosorbent assay (ELISA)

Conditioned media and cell lysates of SH-SY5Y cells treated with phenazopyridine or equivalent vehicle were collected. $A\beta_{1-40}$ and $A\beta_{1-42}$ levels were quantified using ELISA kits (Thermo Fisher Scientific), following the manufacturer's protocols.

Animals and drug delivery

C57BL/6 mice were from Xiamen University Laboratory Animal Center (Xiamen, China). Male APP/PS1 AD model mice were from Model Animal Research Center of Nanjing University (Nanjing, China). Mice were housed 5 per cage in a 24 °C room with a 12-h light/dark cycle. Food and water were supplied ad libitum. All animal experiments were approved by the Animal Experimentation Ethics Committee of Xiamen University and conducted in accordance with the National Institutes of Health Guide for the Care and Use of Laboratory Animals.

Phenazopyridine or equivalent vehicle was directly delivered into the hippocampus of C57BL/6 mice (2 months of age) or intracerebroventricularly infused into the lateral ventricle of male APP/PS1 mice (9 months of age). For intrahippocampal injection, phenazopyridine (15 mg/kg) was injected with a speed of 0.1 μl/min at the following coordinates (from bregma): −2.3 mm posterior, −2.0 mm lateral, and −1.1 mm ventral. For intracerebroventricular infusion, 100 μl of phenazopyridine (125 μg/μl) was infused into the lateral ventricle for 2 weeks using osmotic pumps (RWD Life Science Co., LTD, Shenzhen, China). The osmotic pump was placed underneath the skin at the base of the neck back toward the left hindlimb. The infusion cannula was surgically implanted into the lateral ventricle at the following coordinates (from bregma): −0.5 mm posterior, −1.1 mm lateral, and −2.0 mm ventral.

Behavioral tests

The T-maze test was used to assess short-term working memory. Treated APP/PS1 mice were placed in testing room for at least 1 h before testing to minimize effects of stress on behavior. On the initial trial, mice were placed at the start position located at the end of the stem arm. The door of the stem arm was then raised to allow mice to choose one of the goal arms. Once inside one of the goal arms, the door of that arm was closed and mice were confined there for 30 s. Mice were then placed back at the start position for 5 s. After the stem door was reopened, mice were allowed to choose one of the goal arms again. Procedures were repeated for a total of 11 trials. The percentage of alternations (turns in each goal arm) were counted for comparison.

The fear conditioning test employed electrical foot shock as an unconditioned fear stimulus in conjunction with a tone as a conditioned stimulus. During training, mice were placed into the conditioning chamber

and habituated to their surroundings for 120 s. Following habituation, mice received three pairings between a white noise (80 dB) and a foot shock (2 s, 0.5 mA). The inter-trial interval between each of the pairings was 30 s. Mice were then left in the box for an additional 60 s. On the 2nd day, mice were placed back into the chamber for 10 min in the absence of any stimulus to test context-associated fear conditioning. To assess the auditory-associated fear conditioning, mice were placed back in the same apparatus for 180 s. Subsequently, the white noise was administrated for an additional 180 s and the freezing behavior of mice was recorded.

Brain tissue sample preparation

Brain tissues were harvested 2 days after the behavioral tests. For western blot and quantitative real-time PCR analysis, mice were decapitated and the brains were gently removed. The dissected hippocampi were homogenized in ice-cold RIPA buffer supplemented with protease and phosphatase inhibitor cocktails (Sigma-Aldrich, St. Louis, MO, USA) and were subsequently centrifuged at 12,000 rpm for 20 min at 4 °C. The supernatant was transferred to a new tube and then subjected to protein quantification using a Bradford Protein Assay Kit (Beyotime, Shanghai, China). For Thioflavin-S staining, mice were anesthetized and then perfused with phosphate buffer saline and 4% paraformaldehyde sequentially. The brain was dissected and fixed in 4% paraformaldehyde overnight, followed by immersion in 30% sucrose for 2 days. Coronal sections (35 μm) were obtained by a cryostat (Leica, Buffalo Grove, IL, USA).

Western blot

Equal amounts of proteins were resolved on 10% SDS-PAGE gels and then transferred to polyvinylidene fluoride membranes (Millipore, Bedford, MA). After blocking with 5% non-fat milk, the membranes were incubated with primary antibodies overnight at 4 °C, followed by incubation of appropriate horseradish peroxidase-conjugated secondary antibodies for 1 h at room temperature. The bands were developed by an enhanced chemiluminescence system (Beyotime). Densitometric analyses were carried out by the ImageJ software (National Institutes of Health, Bethesda, MD, USA).

Thioflavin-S staining

Brain sections were incubated in filtered 1 mM Thioflavin-S (dissolved in 50% ethanol) for 8 min at room temperature. Staining was differentiated in 80% ethanol for 15 min, and then washed with three exchanges of distilled water. Sections were coverslipped in aqueous mounting media and visualized under a fluorescence microscope (Olympus, BX51, Tokyo, Japan). Thioflavin-S positive area was analyzed by the ImageJ software (National Institutes of Health, Bethesda, MD, USA).

Chromatin immunoprecipitation (ChIP)

ChIP was performed using a Pierce Agarose ChIP Kit (Thermo Fisher Scientific) following the instructions of the manufacturer. Genomic DNAs from SH-SY5Y cells were incubated with an anti-SMAD3 antibody or control IgG. Immunoprecipitated DNAs were used as templates for PCR, using the following pair of primers: forward, 5′-GGCATCAGACTCCAGGGG-3′; reverse, 5′-TTTTTCTCCATCCCCGCGTC-3′. PCR products were separated on a 2% agarose gel.

Immunofluorescence

Treated cells were rinsed in phosphate buffer saline/Triton-100. After blocking with 5% goat serum for 1 h at room temperature, the cells were incubated with an anti-SMAD3 antibody overnight at 4 °C, with an Alexa Fluor® 594 labeled secondary antibody for 1 h at room temperature, and then with DAPI (to stain the nuclei, 1:1000, Beyotime). The fluorescence was observed under a fluorescence microscope (Olympus).

DNA pull-down and protein mass spectrometry

Approximately 2×10^7 cells were used for the DNA pull-down experiment. The DNA probe (+1167/+1187) and its control (+1167/+1177) labeled with biotin were synthesized by Sangon Biotech. The biotinylated probes were coupled to magnetic beads (Dynabeads™ M-270 Streptavidin, Thermo Fisher Scientific) with gentle rotation for 30 min at room temperature. Beads were washed twice and then incubated with nuclear extracts for 30 min at room temperature with rotation. Beads were collected using a magnetic particle concentrator. Proteins binding to the DNA probes were recovered by boiling, resolved on 10% SDS-PAGE gels, and subjected to silver staining. Gel segments containing proteins specifically pulled down by the +1167/+1187 DNA probe but not by the +1167/+1177 control probe were excised and subjected to in-gel trypsin digestion. Samples were then analyzed on a nanoElute (Bruker, Bremen, Germany) coupled to a timsTOF Pro (Bruker) equipped with a CaptiveSpray source. Peptides were dissolved in 10 μl 0.1% formic acid and auto-sampled directly onto a homemade C18 column (35 cm × 75 μm i.d., 1.9 μm 100 Å). Samples were then eluted for 60 min with linear gradients of 3–35% acetonitrile in 0.1% formic acid at a flow rate of 300 nl/min. Mass spectra data were acquired with a timsTOF Pro mass spectrometer (Bruker) operated in PASEF mode. The raw files were analyzed by the Peaks Studio X software against the Uniprot database.

Statistical analysis

Data were presented as means ± SEM. Significant differences were analyzed using the GraphPad Prism 8 software (GraphPad Software, San Diego, CA, USA). Student's *t* test was used for pairwise comparisons. One-way ANOVA, followed by Bonferroni's test, was used for multiple comparisons. Statistical significance was defined as $p < 0.05$.

RESULTS

Identification and characterization of the human *RPS23RG1* promoter region

We first determined the transcriptional start site (TSS) of the human *RPS23RG1* gene. 5′-RACE was performed using an *RPS23RG1*-specific primer for amplification and cDNAs transcribed from total RNAs of SH-SY5Y, a human neuroblastoma cell line as templates. The 5′-RACE analysis found only one TSS, at 1525 bp upstream of the translation initiation codon. We designated this TSS nucleotide position as "+1" (Fig. 1A). We also carried out 5′-RACE using cDNAs derived from U-87, a human glioma cell line and identified the same TSS (data not shown), implying a uniformity of the *RPS23RG1* TSS in human brain cells. Since the promoter region of a gene typically surrounds the TSS, we assumed a genomic fragment spanning nucleotides −1509 to +1535 relative to the TSS as a full-length *RPS23RG1* promoter region for further analysis (Fig. 1A). No classical TATA or CAAT box was found within the 1.5 Kb distance upstream and downstream the TSS. There were a GC box and a CpG island located between nucleotide position −372 to −367 and +252 to +1017, respectively (Fig. 1A).

To determine the functional promoter region of the human *RPS23RG1* gene, we first generated a series of progressive 5′ deletion fragments of the assumed *RPS23RG1* full-length promoter region and cloned them into a pGL3-basic vector (Fig. 1B). These constructs were transfected into SH-SY5Y cells to study their transcriptional activity. Strikingly, the luciferase activity of all these constructs were lower than the basal activity of the promoterless pGL3-basic vector (Fig. 1B). This raised the possibility that negative cis-element(s) might be present at the 3′-end of the promoter region, leading to the loss of luciferase activity. We therefore generated another series of luciferase reporter constructs containing progressive 3′ deletions of the assumed *RPS23RG1* full-length promoter region (Fig. 1C). The −1509/+1535 and −1509/+1298 constructs still had no luciferase activity. However, the −1509/+1187 construct exhibited moderate, and the −1509/+1127 construct exhibited robust luciferase activity (Fig. 1C), suggesting the presence of negative cis-element(s) between +1127 and +1187 nucleotide position. Moreover, compared to the −1509/+1127 construct, the −1509/+732 and −1509/−506 constructs showed a significant decrease of luciferase activity (Fig. 1C), suggesting that positive regulatory element(s) may be located within the region of +732 to +1127. Indeed, we found that the +732/+1127 domain drove luciferase activity at a nearly comparable level to that of the −1509/+1127 domain, whereas the +732/+1187 domain failed to drive luciferase activity as the +732/+1127 domain did (Fig. 1D).

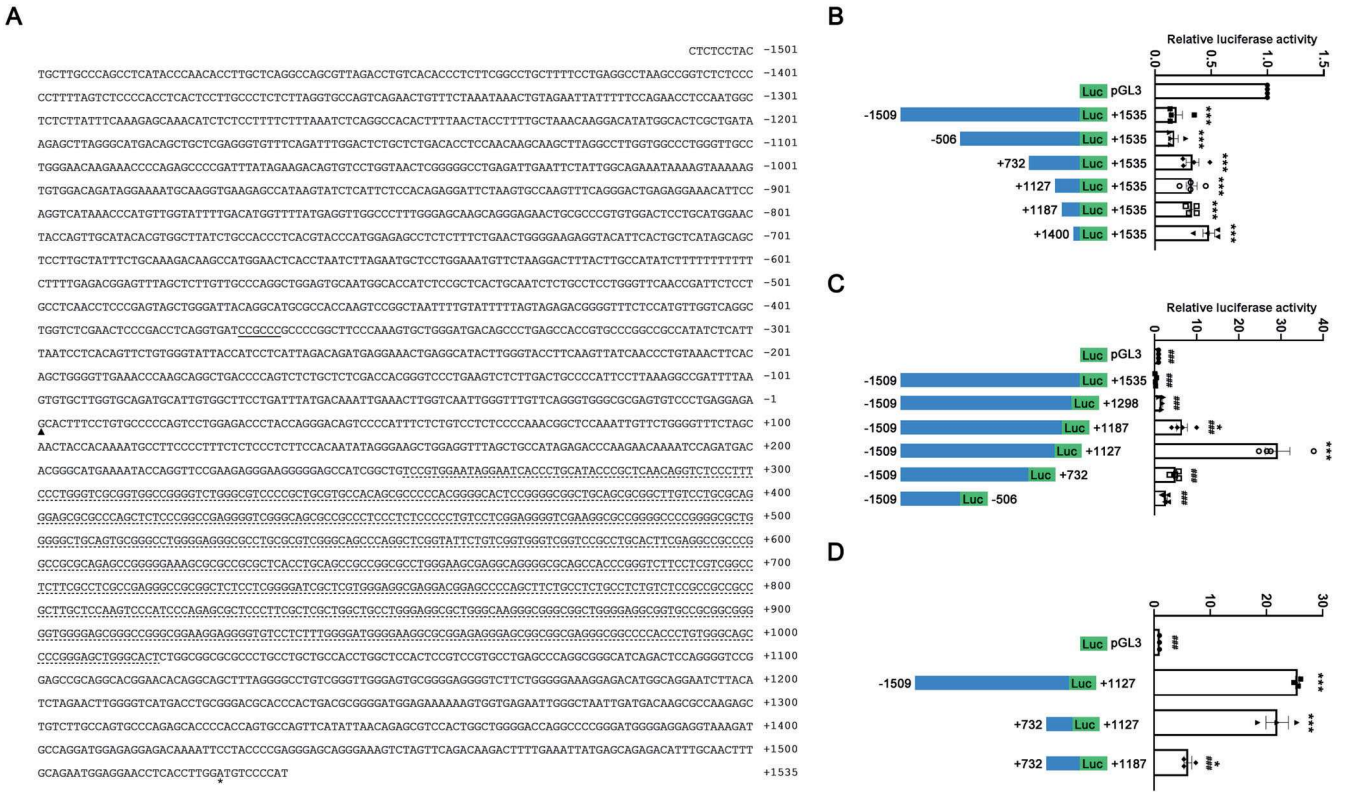

Fig. 1 Characterization of the functional *RPS23RG1* promoter domain. A Nucleotide sequence of the 5-flanking region of human *RPS23RG1* gene. The +1(▲) site denotes the transcription start site (TSS), which was determined by the 5′RACE assay. The translation initiation site is asterisked. A GC box (underlined) and a CpG island (under-dash lined) are shown. The pGL3-basic reporter vectors containing progressive 5′ deletions (**B**) or 3′ deletions (**C**) of an assumed *RPS23RG1* full-length promoter were transiently transfected into SH-SY5Y for 24 h. The pRL reporter plasmid was co-transfected as an internal control to correct the transfection efficiency. One-way ANOVA test; $^{*}p < 0.05$, $^{***}p < 0.001$ for comparisons to the control (pGL3) group; $^{\#\#\#}p < 0.001$ for comparisons to the −1509/+1127 group; $n = 4$. **D** The pGL3-basic reporter vectors containing −1509/+1127, +732/+1127 or +732/+1187 region of the *RPS23RG1* promoter were transiently transfected into SH-SY5Y for 24 h. The pRL reporter plasmid was co-transfected as an internal control to correct the transfection efficiency. One-way ANOVA test; $^{***}p < 0.001$ for comparisons to the control (pGL3) group; $^{\#\#\#}p < 0.001$ for comparisons to the −1509/+1127 group; $n = 3$.

Identification of phenazopyridine as a drug that can promote *RPS23RG1*/*Rps23rg1* transcription

Because increasing RPS23RG1 levels has a potential for AD therapeutics, we wanted to identify drugs that can promote *RPS23RG1* transcription and expression. We generated SH-SY5Y cell lines stably expressing pGL4.17 vectors containing +732/+1127 or +732/+1187 fragments. As expected, the luciferase activity in cells stably expressing +732/+1127 fragment-containing pGL4 vectors (+732/+1127 cell line) were significantly higher than that in cells stably expressing +732/+1187 fragment-containing pGL4 vectors (+732/+1187 cell line) (Fig. 2A). We first used the +732/+1187 cell line to screen 1600 FDA-approved drugs (Fig. 2B, left panel). For the drugs that increased the +732/+1187 cell line luciferase activity by more than 1.1-fold, we used them to treat the 732/+1127 cell line again (Fig. 2B, right panel). The drugs that increased the +732/+1187 cell line luciferase activity by more than 1.2-fold and changed the +732/+1127 cell line luciferase activity with less than 1.1-fold were selected, as we assume that these drugs may antagonize the negative regulatory elements in the *RPS23RG1* gene and thus promote its expression. We identified 18 drugs that fulfills these criteria (Supplementary Table 1). Among them, we found that phenazopyridine treatment induced the highest luciferase activity in the +732/+1187 cell line but only had marginal effect on inducing luciferase activity in the +732/+1127 cell line (Fig. 2B and Supplementary Table 1). In naïve SH-SY5Y cells, we found that phenazopyridine treatments increased the mRNA expression of *RPS23RG1* in a dose-dependent manner (Fig. 2C). Phenazopyridine treatments also promoted *Rps23rg1* mRNA expression in mouse N2a cells (Fig. 2D), suggesting a uniformity of phenazopyridine's effect on promoting *RPS23RG1*/*Rps23rg1* transcription and expression among different species. Moreover, when we intraperitoneally injected phenazopyridine into C57BL/6 mice, we found that phenazopyridine treatments increased *Rps23rg1* levels in lung, liver, and kidney, but not in hippocampal tissues (Fig. 2E). These results suggest that phenazopyridine also promotes *Rps23rg1* expression in vivo, though it may not cross the blood-brain barrier (BBB). When phenazopyridine was directly administered into the mouse hippocampus, an increase of hippocampal *Rps23rg1* expression was indeed observed (Fig. 2F).

Phenazopyridine treatments reduce Aβ levels in vitro

Excess Aβ production and/or reduced Aβ degradation is widely believed to be a primary culprit for AD pathogenesis. Overexpression of RPS23RG1 has been shown to reduce Aβ levels. Therefore, we studied the effect of phenazopyridine on Aβ generation. ELISA analysis showed that the levels of two major Aβ species, $Aβ_{1–40}$ and $Aβ_{1–42}$, were decreased in both SH-SY5Y cells and conditioned media upon phenazopyridine treatments (Fig. 3A–D).

Phenazopyridine treatments ameliorate AD-like phenotypes in APP/PS1 mice

To study whether phenazopyridine has therapeutic potential for AD, we delivered phenazopyridine or vehicle controls into the lateral ventricle of 9-month-old APP/PS1 male mice using osmotic

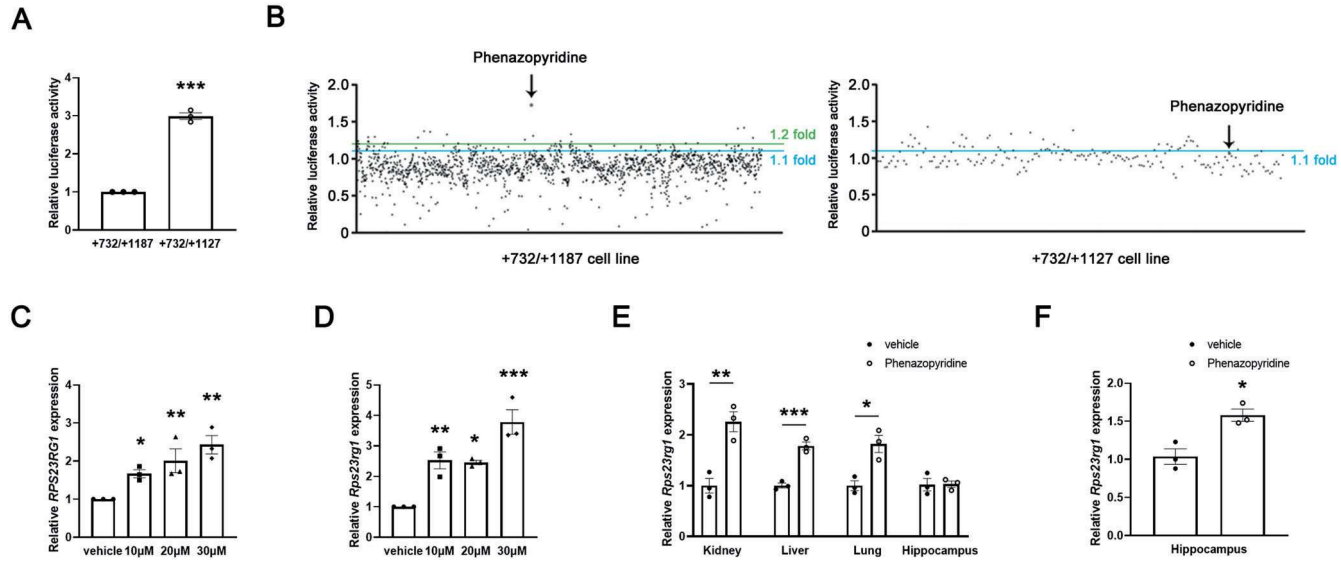

Fig. 2 Phenazopyridine promotes *RPS23RG1*/*Rps23rg1* transcriptional expression. A Same amounts of cell numbers of the +732/+1127 cell line and the +732/+1187 cell line were planted in plates and cultured for 24 h. Luciferase activities in the two cell lines were detected for comparison. Student's *t* test; ***$p < 0.001$; $n = 3$. **B** The +732/+1127 and the +732/+1187 cell lines were treated with vehicle or FAD-approved drugs (10 μM) for 12 h. Luciferase activities in cells treated with individual drugs were normalized to those in cells treated with vehicle. **C** SH-SY5Y and **D** N2a cells were treated with phenazopyridine at indicated concentrations for 12 h. Endogenous human *RPS23RG1* (**C**) and mouse *Rps23rg1* (**D**) mRNA levels were determined by quantitative real-time PCR for comparison. One-way ANOVA test; *$p < 0.05$, **$p < 0.01$, ***$p < 0.001$; $n = 3$. C57BL/6 mice were subjected to intraperitoneal (**E**) or intracerebral (**F**) injection of phenazopyridine (15 mg/kg). 12 h later, *Rps23rg1* mRNA levels in indicated tissues were determined by quantitative real-time PCR for comparison. Student's *t* test; *$p < 0.05$, **$p < 0.01$, ***$p < 0.001$; $n = 3$.

pumps for 2 weeks. Cognitive performance was evaluated by T-maze and fear conditioning tests. In the T-maze test, phenazopyridine-treated APP/PS1 mice showed more spontaneous alternation than vehicle-treated APP/PS1 mice (Fig. 4A). In the fear conditioning test, there was no difference in the freezing time during habituation and conditioning sessions (Fig. 4B). However, phenazopyridine-treated APP/PS1 mice showed significantly increased freezing time during the cue testing session and a trend of increase of the freezing time during the contextual testing session when compared to vehicle-treated mice (Fig. 4B).

Furthermore, we carried out Thioflavin-S staining to detect amyloid plaques in the brain of treated APP/PS1 mice. The results showed that phenazopyridine treatments markedly reduced amyloid plaques compared to the controls (Fig. 4C). Moreover, phenazopyridine treatments increased protein levels of RPS23RG1, PSD-95, and phosphorylated/inactivated GSK-3β, though without affecting levels of tau, phosphorylated tau, and p35 (Fig. 4D). Overall, these results suggest that phenazopyridine treatments can improve some AD-associated cognitive impairments and pathologies in AD model mice through promoting *Rps23rg1* expression.

SMAD3 binds to the *RPS23RG1* promoter and regulates its expression

Since there are negative cis-element(s) between +1127 and +1187 nucleotide positions of the *RPS23RG1* promoter, we further explored the exact genomic domain responsible for *RPS23RG1* expression inhibition. We generated a series of luciferase reporter constructs containing progressive 3′ deletions of the −1509/+1187 region, and found that −1509/+1127, −1509/+1156, −1509/+1167, and −1509/+1177 constructs all exerted much stronger luciferase activity than the −1509/+1187 construct (Fig. 5A), indicating that +1177/+1187 region is responsible for the promoter activity suppression.

To search for transcription factors that can bind to the +1177/+1187 region, SH-SY5Y nuclear lysates were subjected to pull-down using biotinylated +1167/+1187 as a DNA probe. Biotinylated +1167/+1177 was used as a control DNA probe. Bands specifically pulled down by the +1167/+1187 probe but not by the control +1167/+1177 control probe were identified and subjected to mass spectrometry (Supplementary Fig. 1). There were 13 proteins identified (Supplementary Table 2). The known putative binding sites of identified transcription factors were aligned with the sequence spanning nucleotides +1177 to +1187, and a match of a putative SMAD3 binding site was found at the position from +1180 to +1184 (Fig. 5B). When a ChIP assay was carried out using an antibody against SMAD3, amplification of the immunoprecipitates with primers encompassing the +1180/+1184 region resulted in a positive amplification band, confirming that SMAD3 binds to the +1180/+1184 region (Fig. 5C).

Next, we examined the role of SMAD3 in regulating *RPS23RG1* transcription. We found that treatment with the SMAD3 inhibitor SIS3 could increase both the luciferase activity of +732/+1187 (Fig. 5D) and the mRNA levels of endogenous *RPS23RG1* (Fig. 5E). These results demonstrate that SMAD3 binds to the promoter of *RPS23RG1* and suppress its transcription.

To study whether phenazopyridine promotes *RPS23RG1* expression through modulating SMAD3, we treated SH-SY5Y and N2a cells with phenazopyridine and SIS3 individually or collectively. We found that phenazopyridine and SIS3 co-treatment did not significantly increase *RPS23RG1*/*Rps23rg1* expression compared to their individual treatment (Fig. 5F). Moreover, phenazopyridine treatment reduced the binding of SMAD3 to the *RPS23RG1* promoter (Fig. 5G). SMAD3 is an important intracellular mediator of the transforming growth factor-β (TGF-β) signaling pathway. Upon stimulation, SMAD3 can be phosphorylated and translocated to the nucleus and then act as a transcription factor [16–18]. However, although phenazopyridine treatment increased RPS23RG1 protein levels as expected, it had no effects on SMAD3 phosphorylation (Fig. 5H) and nuclear localization (Fig. 5I). These results suggest that phenazopyridine promotes *RPS23RG1* expression possibly through affecting SMAD3 binding to the *RPS23RG1*/*Rps23rg1* promoter without interfering with SMAD3 phosphorylation and nuclear localization.

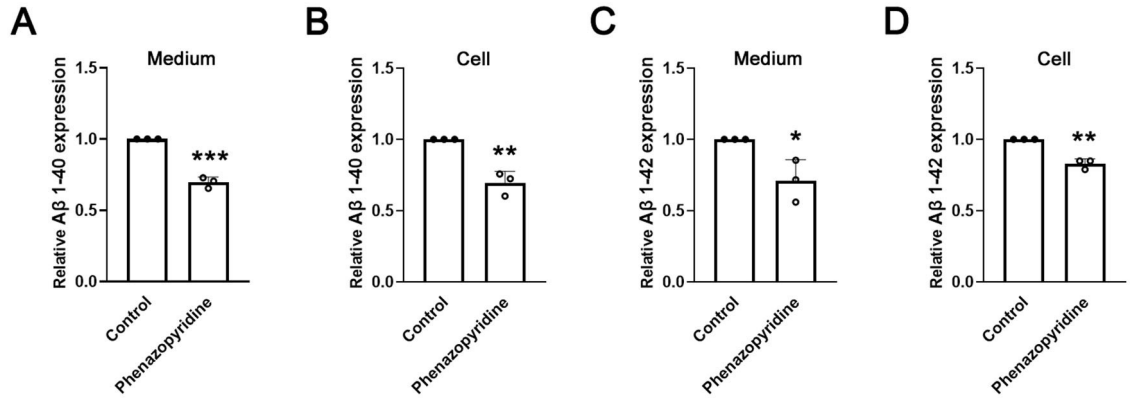

Fig. 3 Phenazopyridine treatment reduces Aβ levels in vitro. A–D SH-SY5Y cells were treated with phenazopyridine (10 μM) for 48 h. Conditioned media (**A**, **C**) and cell lysates (**B**, **D**) were subjected to ELISA to detect $A\beta_{1-40}$ (**A**, **B**) and $A\beta_{1-42}$ (**C**, **D**) levels for comparison. Student's *t* test; $^{*}p < 0.05$, $^{**}p < 0.01$, $^{***}p < 0.001$; $n = 3$.

DISCUSSION

RPS23RG1 can decrease Aβ levels and tau hyperphosphorylation and alleviate synaptic and cognitive deficits in AD cellular and animal models [11, 12, 14, 15]. Therefore, upregulation of RPS23RG1 expression may be a potential therapeutic approach for AD treatment. In the present study, we investigated the transcription regulation of *RPS23RG1* for the first time. One *RPS23RG1* TSS (+1) was identified in SH-SY5Y cells. Although no typical regulatory elements were predicted around the TSS, a CpG island was found in the +252 to +1017 region, which partially overlapped with the positive regulatory region (+732 to +1127) and was upstream of the negative regulatory region (+1127 to +1187). These data suggest that the essential promoter region of *RPS23RG1* locates at ~1 kb downstream of the TSS. Moreover, the promoter activities of the assumed full-length and 5′ deleted *RPS23RG1* promoter domains were very low, suggesting that the negative regulatory region has a dominant role in transcription. This is consistent with our observation that endogenous *RPS23RG1*/*Rps23rg1* expression is low under most conditions and further decreased during AD progression [12, 15]. Therefore, there is a great potential to promote *RPS23RG1* expression.

We generated a reporter system to screen compounds that may increase *RPS23RG1* expression through antagonizing negative regulatory elements within the +1127/+1187 region, based on the rationale that such compounds should promote luciferase activity in the +732/+1187 cell line but not in the +732/+1127 cell line. This screening strategy excludes compounds that may promote *RPS23RG1* expression through strengthening the positive regulatory elements, which need to be evaluated in the future. Nevertheless, using the current screening strategy, we identified one positive drug, phenazopyridine from FDA-approved drugs screened here. Phenazopyridine is clinically used for treating urinary tract pain and its possible mechanism of action is to function as a local analgesic or anesthetic on the mucosa of the urinary tract [19, 20]. However, the role of phenazopyridine in central nervous system diseases has not been explored yet. Herein, we demonstrated that phenazopyridine not only promoted *RPS23RG1*/*Rps23rg1* expression, but also reduced Aβ levels in cell culture and attenuated Aβ plaques and cognitive impairments in APP/PS1 mice. Interestingly, one recent study indicated that phenazopyridine could bind to Aβ, raising the possibility of phenazopyridine being an Aβ aggregation inhibitor [21]. Therefore, although our in vitro study indicates that phenazopyridine reduces Aβ generation through promoting *RPS23RG1* expression, it is possible that phenazopyridine exerts its protection in vivo through both promoting *Rps23rg1* expression and interacting with Aβ to inhibit its aggregation; and this deserves further scrutiny.

Phenazopyridine treatments also increased PSD-95 and phosphorylated/inactivated GSK-3β levels as expected, but did not affect p35 levels and tau phosphorylation in vivo. The APP/PS1 mouse line is primarily used to study amyloid pathologies of AD [22, 23]. Although phosphorylated tau immunoreactivity was seen in the cell bodies of CA3 hippocampal neurons of 16-month old APP/PS1 mice [24], our western blotting results found that tau phosphorylation was not significantly different between APP/PS1 and WT mice at 8 months of age (Supplementary Fig. 2). Therefore, it is possible that the reason phenazopyridine treatment did not affect tau phosphorylation in our current study is that the studied mice were not old enough to develop tau pathologies. Further studies using animal models exhibiting tau pathologies shall help determine the effect of phenazopyridine on tau. Nevertheless, phenazopyridine has a potential to reduce Aβ deposition and treat Aβ deposition-related diseases such as AD and cerebral amyloid angiopathy. Whether phenazopyridine may reduce tau pathologies in tauopathy requires additional investigation.

We furthered determined +1177/+1187 as a critical negative regulatory domain of *RPS23RG1*. We found that the transcription factor SMAD3 bound to this region and SMAD3 inhibition promoted *RPS23RG1* expression. SMAD3 is an important intracellular mediator of the TGF-β signaling pathway and regulates multiple cellular processes such as cell cycle, tumor suppression, and inflammation [17, 18]. TGF-β levels are increased and subcellular localizations of phosphorylated SMAD3 are altered in human AD brain tissues [25, 26]. However, although reducing neuronal TGF-β signaling promoted neurodegeneration and AD-like pathologies [27], inhibiting TGF-β-SMAD2/3 signaling in peripheral macrophages attenuated AD-like pathologies [28]. More recently, treatments with the SMAD3 inhibitor SIS3 were also shown to attenuate Aβ plaques, neuroinflammation, and cognitive impairments in APP/PS1 mice probably through enhancing Aβ clearance by peripheral macrophages [29]. Herein, we found that SIS3 treatments promoted *RPS23RG1* expression. Since RPS23RG1 is ubiquitously expressed in a variety of cells such as neurons, microglia, and astrocytes, whether RPS23RG1 also modulates neuroinflammation and whether SMAD3 inhibition also exerts neuroprotection against AD through regulating *RPS23RG1* expression deserve further scrutiny.

Phenazopyridine was identified through screening compounds that antagonize *RPS23RG1* negative regulatory elements and SMAD3 was identified to bind to the core *RPS23RG1* negative regulatory elements. Herein, we found that phenazopyridine could not further increase *RPS23RG1*/*Rps23rg1* expression when SMAD3 was inhibited by SIS3. Moreover, phenazopyridine treatment

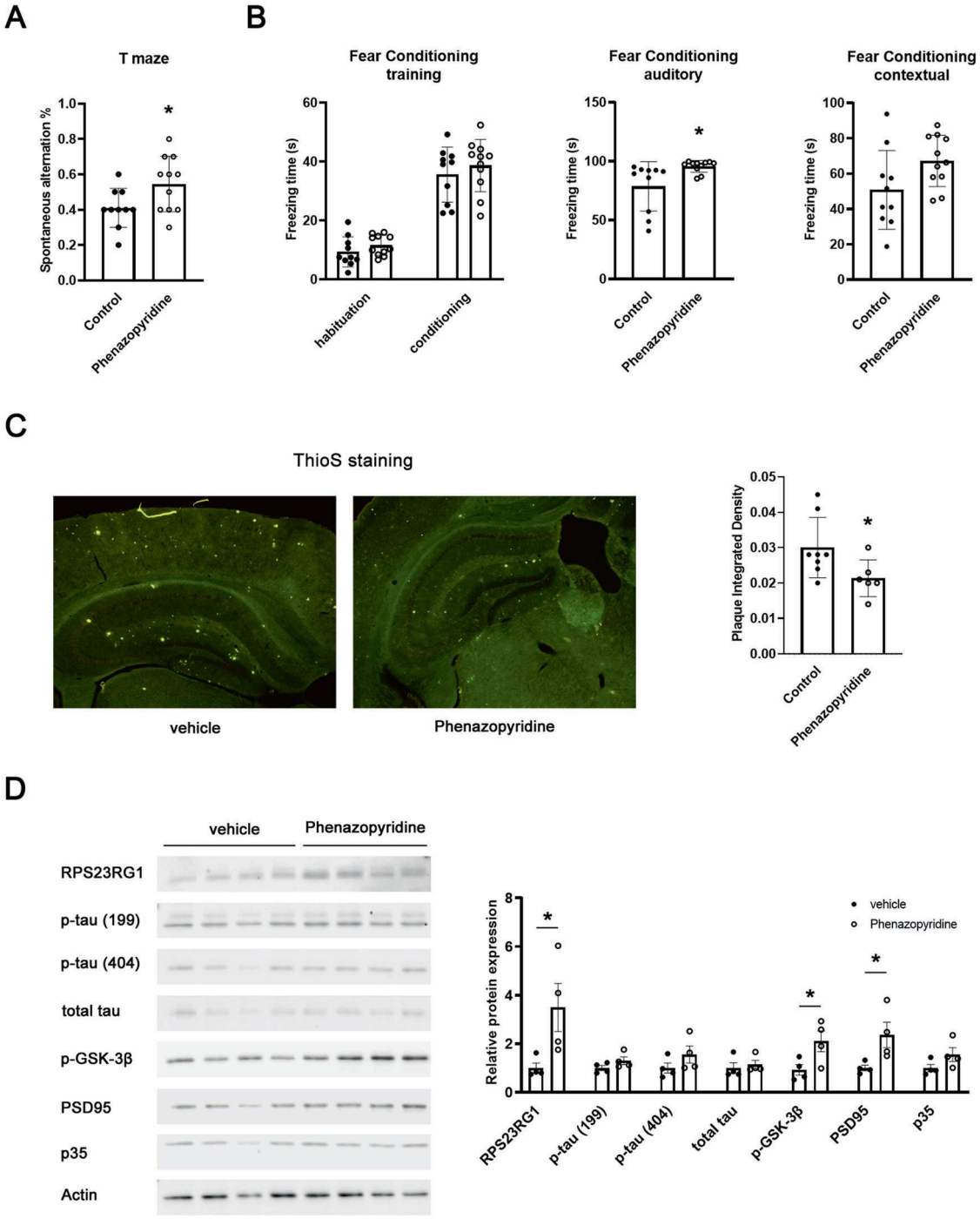

Fig. 4 Phenazopyridine treatment improves memory and attenuates AD-associated pathologies in APP/PS1 mice. APP/PS1 mice treated with phenazopyridine or vehicle control were subjected to memory tests using the T-maze test to compare their spontaneous alternation percentages (**A**), and the fear conditioning test to compare their freezing times upon giving auditory cues or contextual cues (**B**). Student's *t* test; $*p < 0.05$; $n = 10$ for phenazopyridine-treated mice, $n = 11$ for control mice. **C** Treated mice were sacrificed and brain sections were stained with Thioflavin-S (ThioS) to show Aβ plaques. Aβ plaque density in the hippocampus was quantified for comparison. Student's *t* test; $*p < 0.05$; $n = 6$ for phenazopyridine-treated mice, $n = 8$ for control mice. **D** Hippocampal tissues from treated APP/PS1 mice were dissected and subjected to western blot analysis to study indicated proteins. Protein levels were quantified and normalized to those of Actin form comparisons. Student's *t* test; $*p < 0.05$; $n = 4$ for each group. Filled circles represent control mice; blank circles represent phenazopyridine-treated mice.

reduced the binding of SMAD3 to the core *RPS23RG1* negative regulatory elements. These results suggest that phenazopyridine regulates *RPS23RG1* expression through modulating the function of SMAD3. However, although SMAD3 is classically activated by phosphorylation and subsequent nuclear translocation [16], we did not observe changes in SMAD3 phosphorylation and nuclear localization upon phenazopyridine treatment. Therefore, phenazopyridine may inhibit SMAD3 function by interfering with the

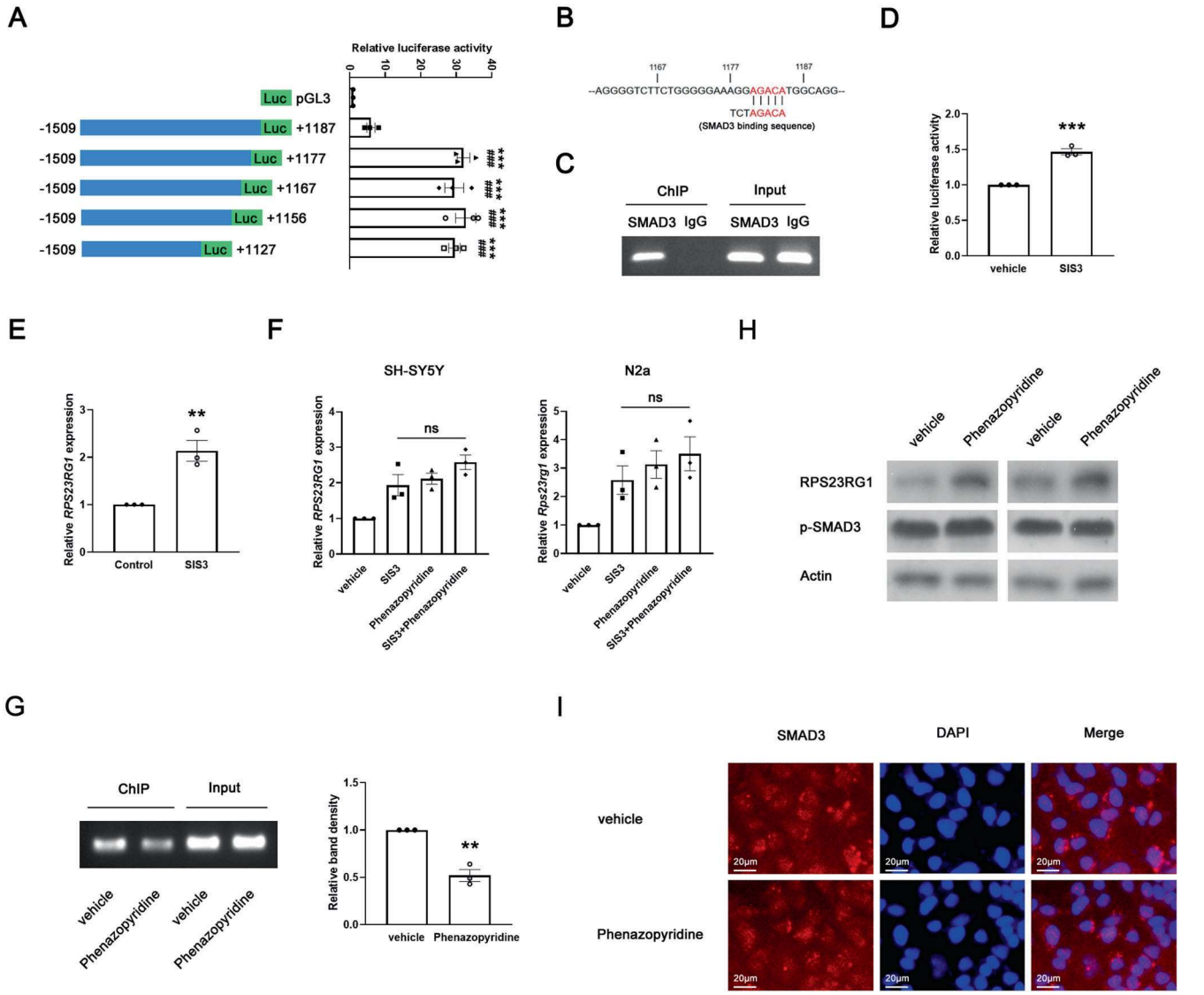

Fig. 5 SMAD3 binds to the promoter of *RPS23RG1* and regulates its expression. A The pGL3-basic reporter vectors containing progressive 3′ deletions of the *RPS23RG1* promoter were transiently transfected into SH-SY5Y for 24 h. The pRL reporter plasmid was co-transfected as an internal control to correct the transfection efficiency. One-way ANOVA; $^{***}p < 0.001$ for comparisons to the control (pGL3) group; $^{\#\#\#}p < 0.001$ for comparisons to the −1509/+1187 group; $n = 3$. **B** A putative SMAD3 binding site was found at the +1180 to +1184 positions of the *RPS23RG1* promoter. **C** ChIP assays were used to pulled down SMAD3 bound genomic DNAs using an antibody against SMAD3 or normal IgG (as a negative control). PCR was performed using immunoprecipitated DNAs or input DNAs as templates. PCR products were separated on a 2% agarose gel. **D** The +732/+1187 cell line was treated with SIS3 (10 μM) for 12 h. Then luciferase activity was quantified for comparison. Student's *t* test; $^{***}p < 0.001$; $n = 3$. **E** SH-SY5Y cells were treated with SIS3 (10 μM) for 12 h. Endogenous *RPS23RG1* mRNA levels were determined. Student's *t* test; $^{**}p < 0.01$; $n = 3$. **F** SH-SY5Y and N2a cells were treated with phenazopyridine and SIS3 individually or collectively for 12 h. Human *RPS23RG1* and mouse *Rps23rg1* mRNA levels were determined by quantitative real-time PCR for comparison. One-way ANOVA test; $^{*}p < 0.05$, ns not significant; $n = 3$. **G** SH-SY5Y cells were treated with phenazopyridine for 12 h. ChIP assays were performed using an antibody against SMAD3. PCR was performed using immunoprecipitated DNAs or input DNAs as templates. PCR products were separated on a 2% agarose gel. PCR band intensities were quantified and normalized to those of inputs for comparison. $^{**}p < 0.01$; $n = 3$. **H** N2a cells were treated with phenazopyridine for 12 h and then subjected to western blot analysis to determine RPS23RG1 and p-SMAD3 levels. Actin was used as a loading control. **I** SH-SY5Y cells were treated with phenazopyridine for 12 h. The localization of SMAD3 (in red) was detected by immunofluorescence. DAPI was used to stain the nuclei (in blue). Scale bars: 20 μm.

binding of SMAD3 to the *RPS23RG1* promoter directly or indirectly through affecting SMAD3 co-factors. For example, SMAD3 is known to cooperate with AP-1 transcription factors to mediate TGF-β-induced transcription [30].

In summary, we have characterized the promoter region of the *RPS23RG1* gene that is closely associated with AD and demonstrated that SMAD3 negatively regulates *RPS23RG1* expression. Moreover, we have identified phenazopyridine as a drug that can promote *RPS23RG1/Rps23rg1* expression and attenuate Aβ pathologies and cognitive impairments in APP/PS1 AD model mice. Although it appears that phenazopyridine does not cross the BBB, delivery through the intranasal route and intrathecal injection, and uses of appropriate packaging vehicles such as nanoparticles and extracellular vesicles may help bypass this limitation [31, 32]. Together, our results provide new avenues for AD therapeutics through targeting RPS23RG1.

REFERENCES

1. Rahman MM, Lendel C. Extracellular protein components of amyloid plaques and their roles in Alzheimer's disease pathology. Mol Neurodegener. 2021;16:59.
2. Hanseeuw BJ, Betensky RA, Jacobs HIL, Schultz AP, Sepulcre J, Becker JA, et al. Association of amyloid and tau with cognition in preclinical Alzheimer disease: a longitudinal study. JAMA Neurol. 2019;76:915–24.
3. Guo T, Zhang D, Zeng Y, Huang TY, Xu H, Zhao Y. Molecular and cellular mechanisms underlying the pathogenesis of Alzheimer's disease. Mol Neurodegener. 2020;15:40.
4. O'Brien RJ, Wong PC. Amyloid precursor protein processing and Alzheimer's disease. Annu Rev Neurosci. 2011;34:185–204.
5. Shankar GM, Li S, Mehta TH, Garcia-Munoz A, Shepardson NE, Smith I, et al. Amyloid-beta protein dimers isolated directly from Alzheimer's brains impair synaptic plasticity and memory. Nat Med. 2008;14:837–42.
6. Dahlgren KN, Manelli AM, Stine WB Jr, Baker LK, Krafft GA, LaDu MJ. Oligomeric and fibrillar species of amyloid-beta peptides differentially affect neuronal viability. J Biol Chem. 2002;277:32046–53.
7. Xia Y, Prokop S, Giasson BI. "Don't Phos Over Tau": recent developments in clinical biomarkers and therapies targeting tau phosphorylation in Alzheimer's disease and other tauopathies. Mol Neurodegener. 2021;16:37.
8. Seto M, Weiner RL, Dumitrescu L, Hohman TJ. Protective genes and pathways in Alzheimer's disease: moving towards precision interventions. Mol Neurodegener. 2021;16:29.
9. 2020 Alzheimer's disease facts and figures. Alzheimers Dement. 2020;16:391–460.
10. McDade E, Llibre-Guerra JJ, Holtzman DM, Morris JC, Bateman RJ. The informed road map to prevention of Alzheimer disease: a call to arms. Mol Neurodegener. 2021;16:49.
11. Zhang YW, Liu S, Zhang X, Li WB, Chen Y, Huang X, et al. A functional mouse retroposed gene Rps23r1 reduces Alzheimer's beta-amyloid levels and tau phosphorylation. Neuron. 2009;64:328–40.
12. Zhao D, Meng J, Zhao Y, Huo Y, Liu Y, Zheng N, et al. RPS23RG1 is required for synaptic integrity and rescues Alzheimer's disease-associated cognitive deficits. Biol Psychiatry. 2019;86:171–84.
13. Huang X, Chen Y, Li WB, Cohen SN, Liao FF, Li L, et al. The Rps23rg gene family originated through retroposition of the ribosomal protein s23 mRNA and encodes proteins that decrease Alzheimer's beta-amyloid level and tau phosphorylation. Hum Mol Genet. 2010;19:3835–43.
14. Zhao D, Zhou Y, Huo Y, Meng J, Xiao X, Han L, et al. RPS23RG1 modulates tau phosphorylation and axon outgrowth through regulating p35 proteasomal degradation. Cell Death Differ. 2021;28:337–48.
15. Yan L, Chen Y, Li W, Huang X, Badie H, Jian F, et al. RPS23RG1 reduces Abeta oligomer-induced synaptic and cognitive deficits. Sci Rep. 2016;6:18668.
16. Attisano L, Wrana JL. Signal transduction by the TGF-beta superfamily. Science. 2002;296:1646–7.
17. Tang PM, Nikolic-Paterson DJ, Lan HY. Macrophages: versatile players in renal inflammation and fibrosis. Nat Rev Nephrol. 2019;15:144–58.
18. Tarasewicz E, Jeruss JS. Phospho-specific Smad3 signaling: impact on breast oncogenesis. Cell Cycle. 2012;11:2443–51.
19. Zelenitsky SA, Zhanel GG. Phenazopyridine in urinary tract infections. Ann Pharmacother. 1996;30:866–8.
20. Gaines KK. Phenazopyridine hydrochloride: the use and abuse of an old standby for UTI. Urol Nurs. 2004;24:207–9.
21. McClure R, Redha R, Vinson P, Pham W. A robust and scalable high-throughput compatible assay for screening amyloid-beta-binding compounds. J Alzheimers Dis. 2019;70:187–97.
22. Drummond E, Wisniewski T. Alzheimer's disease: experimental models and reality. Acta Neuropathol. 2017;133:155–75.
23. Sasaguri H, Hashimoto S, Watamura N, Sato K, Takamura R, Nagata K, et al. Recent advances in the modeling of Alzheimer's disease. Front Neurosci. 2022;16:807473.
24. Malm TM, Iivonen H, Goldsteins G, Keksa-Goldsteine V, Ahtoniemi T, Kanninen K, et al. Pyrrolidine dithiocarbamate activates Akt and improves spatial learning in APP/PS1 mice without affecting beta-amyloid burden. J Neurosci. 2007;27:3712–21.
25. Flanders KC, Lippa CF, Smith TW, Pollen DA, Sporn MB. Altered expression of transforming growth factor-beta in Alzheimer's disease. Neurology. 1995;45:1561–9.
26. Ueberham U, Ueberham E, Gruschka H, Arendt T. Altered subcellular location of phosphorylated Smads in Alzheimer's disease. Eur J Neurosci. 2006;24:2327–34.
27. Tesseur I, Zou K, Esposito L, Bard F, Berber E, Can JV, et al. Deficiency in neuronal TGF-beta signaling promotes neurodegeneration and Alzheimer's pathology. J Clin Invest. 2006;116:3060–9.
28. Town T, Laouar Y, Pittenger C, Mori T, Szekely CA, Tan J, et al. Blocking TGF-beta-Smad2/3 innate immune signaling mitigates Alzheimer-like pathology. Nat Med. 2008;14:681–7.
29. Xu L, Pan CL, Wu XH, Song JJ, Meng P, Li L, et al. Inhibition of Smad3 in macrophages promotes Abeta efflux from the brain and thereby ameliorates Alzheimer's pathology. Brain Behav Immun. 2021;95:154–67.
30. Zhang Y, Feng XH, Derynck R. Smad3 and Smad4 cooperate with c-Jun/c-Fos to mediate TGF-beta-induced transcription. Nature. 1998;394:909–13.
31. Terstappen GC, Meyer AH, Bell RD, Zhang W. Strategies for delivering therapeutics across the blood-brain barrier. Nat Rev Drug Disco. 2021;20:362–83.
32. Mansor NI, Nordin N, Mohamed F, Ling KH, Rosli R, Hassan Z. Crossing the blood-brain barrier: a review on drug delivery strategies for treatment of the central nervous system diseases. Curr Drug Deliv. 2019;16:698–711.

AUTHOR CONTRIBUTIONS

CW and YwZ designed research. CW and YZ carried out most molecular and animal studies. DZ, YH, and JX performed some molecular experiments. XZ and HL provided technical support. HX helped on data interpretation. YwZ supervised the project. CW and YwZ wrote the manuscript. All authors reviewed and approved the final paper.

FUNDING

This work was supported by grants from National Natural Science Foundation of China (82130039 and U21A20361 to YwZ; 82001442 to DZ, and 92049202 and 92149303 to HX), National Key Research and Development Program of China (2018YFC2000400 to YwZ), and The Major Program of Brain Science and Brain-Like Intelligence Technology (2021ZD0202400 to HX).

COMPETING INTERESTS

The authors declare no competing interests.

ADDITIONAL INFORMATION

Supplementary information The online version contains supplementary material available at https://doi.org/10.1038/s41386-022-01373-7.

Correspondence and requests for materials should be addressed to Chong Wang or Yun-wu Zhang.